

Results from the LSND Neutrino Oscillation Search for $\bar{\nu}_\mu \longrightarrow \bar{\nu}_e$

James E. Hill

University of Pennsylvania

(June 19, 2017)

Abstract

The Liquid Scintillator Neutrino Detector (LSND) at the Los Alamos Meson Physics Facility sets bounds on neutrino oscillations in the appearance channel $\bar{\nu}_\mu \rightarrow \bar{\nu}_e$ by searching for the signature of the reaction $\bar{\nu}_e p \rightarrow e^+ n$: an e^+ followed by a 2.2MeV gamma ray from neutron capture. Five $e^\pm\text{-}\gamma$ coincidences are observed in time with the LAMPF beam, with an estimated background of 6.2 events. The 90% confidence limits obtained are: $\Delta m^2 < 0.07\text{eV}^2$ for $\sin^2 2\theta = 1$, and $\sin^2 2\theta < 6 \cdot 10^{-3}$ for $\Delta m^2 \gtrsim 20\text{eV}^2$.

arXiv:hep-ex/9504009v1 25 Apr 1995

The phenomenon of neutrino oscillations [1] is a sensitive probe of finite masses in the neutral lepton sector, the only remaining elementary fermions with unknown masses. With a few simplifying assumptions, the probability, P , of oscillations $\bar{\nu}_\mu \longrightarrow \bar{\nu}_e$ can be written $P_{\bar{\nu}_\mu \rightarrow \bar{\nu}_e} = \sin^2(2\theta) \sin^2 \{1.27\Delta(m^2(\text{eV}^2))L(\text{m})/E(\text{MeV})\}$. Experiments at accelerators may probe very low, ($\mathcal{O}(10^{-3})$) values of the mixing strength, $\sin^2 2\theta$, and mass splittings $\Delta m^2 \approx |m_{\bar{\nu}_\mu}^2 - m_{\bar{\nu}_e}^2| \gtrsim \mathcal{O}(10^{-2}\text{eV}^2)$ by searches for appearance of $\bar{\nu}_e$ in a high intensity $\bar{\nu}_\mu$ beam.

The Liquid Scintillator Neutrino Detector (LSND) was built at the Los Alamos Meson Physics Facility (LAMPF) in part to search for oscillations $\bar{\nu}_\mu \longrightarrow \bar{\nu}_e$. The $\bar{\nu}_e$ is detected via the weak charged current interaction $\bar{\nu}_e p \rightarrow e^+ n$. For $\bar{\nu}_e$ resulting from the $\bar{\nu}_\mu$ from muon decay at rest, this interaction will produce a continuous positron spectrum up to 50MeV, which can be loosely tagged by a delayed time coincidence with the 2.2MeV γ ray emitted after neutron capture on hydrogen in the detector mineral oil. Since the detector is insensitive to the charge of a particle, the search is performed above the 35MeV endpoint of the abundant reaction $\nu_e \text{ }^{12}\text{C} \rightarrow e^- \text{ }^{12}\text{N}$.

LAMPF produces neutrinos from the decay of pions and muons. The predominant processes are $\pi^+ \rightarrow \mu^+ \nu_\mu$ and $\mu^+ \rightarrow e^+ \bar{\nu}_\mu \nu_e$, the decay of negative particles being suppressed by the high probability of nuclear capture. Measured pion cross sections, [2] are used in the neutrino beam simulation, [3] which predicts a total flux of $\bar{\nu}_\mu$ from μ decay at rest of $3 \cdot 10^{13} \bar{\nu}_\mu / \text{cm}^2$ at the center of LSND for the 3.5 months of data analyzed, with an estimated absolute uncertainty of 7% and $\Phi_{\bar{\nu}_e} / \Phi_{\bar{\nu}_\mu} \approx 4 \cdot 10^{-4}$. The neutrino beam also allows a search for $\nu_\mu \longrightarrow \nu_e$ oscillations [4] and ν_μ quasielastic interactions [5,6] because a few percent of π^+ decay in flight giving a directed beam of higher momentum ν_μ . Data for that search are not analyzed here, but the high energy ν_μ contribute to a potential background source.

The detector is an approximately cylindrical tank 8.3m long and 5.7m in diameter, 29.8m from the beam production point. Inside the tank, 1220 8" Hamamatsu phototubes (PMT) provide 25% uniform areal coverage of 157m³ of mineral oil doped with a small amount, 0.031 g/l, of butyl-PBD scintillator. The tank is surrounded except on the bottom by a

high light output liquid scintillator veto shield [7] viewed by 292 5" PMT which detects high energy cosmic ray muons with a measured inefficiency of $\sim 2 \cdot 10^{-5}$. The entire apparatus is under $\sim 2000\text{g/cm}^2$ of passive shielding. A sample of $\mathcal{O}(10^6)$ electrons from cosmic ray muon decay is used to determine the energy response and resolution of the detector, as well as the efficiency of e^\pm identification. The fractional energy resolution for electrons at 53MeV is 8%, and at 35MeV is 10%. A lower cut on energy of 37MeV is applied to e^\pm signal candidates.

Triggering decisions are based on global sums over 200ns of detector and of veto shield PMT signal multiplicities. Events with more than 5 veto PMT signals are vetoed and initiate a veto of future events for $15.2\mu\text{s}$. If not vetoed, any event passing a threshold corresponding to 5MeV electron energy in the detector is designated a primary trigger, and recorded with up to four events in the previous $52\mu\text{s}$ that passed a threshold of 17 detector, or 5 veto PMT signals. Unvetoed primaries with ≥ 125 detector PMT signals initiate a lowering of the primary threshold to 21 detector PMT for the next millisecond so that subsequent low energy gamma radiation can be detected. Event losses due to the veto shield and to the loss of events overwritten in memory total $19 \pm 3\%$ for primaries, and 22% for gamma rays.

The beam status is not used in trigger decisions, but recorded with each event. This allows beam-unrelated backgrounds to be characterized in detail. The number expected is predictable with good precision because of the 7.6% ratio of beam-on time to beam-off time, and the spatial distribution of this background aids in distinguishing it from the potential signal. Particle identification is accomplished by detection of forward directed prompt light in the Čerenkov cone of relativistic particles, distinguishing them from heavier charged particles which produce isotropic, more slowly emitted scintillation light. Light and heavy particles are distinguished well by the $\chi^2/\text{d.f.}$ for the reconstructed track direction fit, the $\chi^2/\text{d.f.}$ for the fit to the vertex position, and the fraction of PMT signals occurring (corrected for photon time of flight) more than 12ns later than the reconstructed event time. This product is corrected for an observed energy dependence based on studies of the cosmic ray muon decay electron sample. Selection based on this parameter is 89% efficient

in accepting e^\pm and 99% efficient in rejecting heavy backgrounds.

LSND took data for 6 weeks in a preliminary run in 1993, with a $\bar{\nu}_\mu$ flux of $9 \cdot 10^{12} \nu/\text{cm}^2$, after which the configuration of the active veto system was slightly changed, the last of the passive shielding was added, and the electronics were modified to linearize the energy response of the detector. This change in the energy response changes the energy dependence of the particle identification scheme, contributing to the incompatibility of the data from the early run and the $3.5\times$ larger data set from a 1994 run. Only 1994 data are used in this analysis.

The properties of neutron capture gamma rays can be studied using the large flux of cosmic ray neutrons and the $186\mu\text{s}$ capture time of neutrons in mineral oil. Requirements are placed on the energy of gamma rays, their time of occurrence and distance relative to the e^\pm . It is required that the reconstructed relative distance be less than 2.4m (The reconstruction error on gamma rays is approximately 1m.), the relative time less than $750\mu\text{s}$ (≈ 4 capture times), and that the gamma-ray exhibit at least 26 detector PMT hits. The efficiency for the detection of a capture gamma-ray from a neutron coming from a signal event is 60%. (See Table II for the individual efficiencies.) The measured probability of an accidental $e^\pm-\gamma$ coincidence passing the selection criteria is 12%.

Scatter plots of the projections of the reconstructed positions of background (*i.e.* beam-off) events are shown in Fig. 1. There are 1381 e^\pm shown in the top plots, and 1961 associated gamma-rays shown directly below them. No $e^\pm-\gamma$ coincidence is required in the data of Fig. 1 (except the 1ms trigger requirement), and the spatial requirement is only that the reconstructed e^\pm be at least 30cm from the surface defined by the PMT faces. The coordinate system is defined by taking \hat{z} along the detector cylindrical axis and \hat{y} vertical; the beam is along $-0.1\hat{y} + 0.99\hat{z}$. Both Y-X and Y-Z projections are shown. The surface at the PMT faces is represented by the plot frame in the Y-Z projections, and by the thin curve and part of the frame in the Y-X plots.

Figure 2 shows the same distributions for all (142) e^\pm in time with the beam that pass all the final e^\pm selection criteria except a later, tighter fiducial volume requirement, and all (189)

gamma rays associated with these e^\pm . These events are the exact beam-on complement of those shown in Fig. 1. Any $\bar{\nu}_\mu \rightarrow \bar{\nu}_e$ oscillation signal must emerge from the events in Fig. 2, after the background indicated in Fig. 1 is properly subtracted, and an $e^\pm\text{-}\gamma$ coincidence required.

The inhomogeneity of the background in Fig. 1 and of the potential signal in Fig. 2 requires confining the fiducial volume to a region of the detector which is not only more background free, but within which there are no strong gradients of event density. Since the backgrounds for both e^\pm and for coincident γ are inhomogeneous, and both enhanced at the bottom of the detector, the distribution of distance between primaries and accidentally coincident gamma rays will not be constant throughout the detector. This problem is addressed both by tightening the region analyzed, and by the requirement that coincidences pass each of the separate criteria on $e^\pm\text{-}\gamma$ relative time and distance, and gamma ray energy. A region is chosen, in part from the data in Figs. 1 and 2, and in part from separate measurements of the spatial dependence of e^\pm detection efficiency, which limits the search to approximately 59m^3 of active volume. The volume shown in Figs. 1 and 2 is reduced by 3/4 by moving inward from 30cm to 50cm from the PMT faces, and by a similar factor by excluding 1m at the bottom of the remaining region.

Figure 3a shows the e^\pm positions for the subset of the beam-on events in Fig. 2 with a nominally coincident 2.2MeV gamma-ray. All of the events shown in Fig. 2 that satisfy the $e^\pm\text{-}\gamma$ coincidence requirement are included in Fig. 3a. Within the fiducial volume (dotted line) five events remain as possible signal candidates. Four events are concentrated just outside the periphery of the fiducial volume, and 16 near the bottom of the detector in 1/3 of the total volume analyzed.

Figure 3b shows the energy spectrum of the events in Fig. 3a; the five events within the fiducial volume are in the shaded portion of the plot. 43 events pass all the same requirements while the beam is off, implying a background from beam-unrelated sources of $(43 \times 0.076 =) 3.3 \pm 0.49(\text{stat}) \pm 0.04(\text{sys.})$ events. Almost as large in number is the class of events with neutrino induced e^- in the correct energy range in accidental coincidence

with low energy gamma radiation in the detector. These include $\nu_\mu e \rightarrow \nu_\mu e$ and $\nu_e e \rightarrow \nu_e e$, $\nu_e {}^{13}\text{C} \rightarrow e^- {}^{13}\text{N}$, with an endpoint of about 50MeV, and $\nu_\mu {}^{12}\text{C} \rightarrow \mu^- X$ (from higher energy neutrinos from pion decay in flight) where the muon is undetected. There are also expected to be e^- from $\nu_e {}^{12}\text{C} \rightarrow e^- {}^{12}\text{N}$ which have energy measured within 1σ of the reaction endpoint of 35MeV. The excess of e^\pm (beam-on - beam-off) satisfying all the e^\pm selection criteria, but without a coincident gamma-ray is made up of these events (without an accidental gamma-ray) plus any beam related e^\pm missing a real gamma-ray coincidence. Both the accidental coincidence probability and the beam excess of neutrino-induced e^\pm are measured. The background from beam induced e^\pm in accidental coincidence with a gamma ray is calculated from these measurements as 2.5 ± 0.9 . There is an expected background of events from $\bar{\nu}_e$ contamination from μ^- decay in the beam stop of about 0.3 events. Other backgrounds have been calculated, and are all found to be relatively low.

These results are stable against variation of the above selection requirements. For example, extending the region analyzed to $y = -100\text{cm}$, *i.e.* 50cm lower (≈ 1.2 times the fiducial volume above) leaves 7 beam-on events with a background of 8.7 events. Similarly, tightening the requirement on the $e-\gamma$ relative distance to 1m (from 2.4m) leaves only 2 beam-on events with a background of 1.5, or, setting the limit on relative time to 375 (from 750 μs) leaves 1 event with a background of 3.5.

Major backgrounds are summarized in Table II. The total background of 6.2 events leaves no apparent signal for $\bar{\nu}_\mu \rightarrow \bar{\nu}_e$ oscillations. The resulting limits on the oscillation parameters Δm^2 and $\sin^2 2\theta$ based on this number of events are shown in Fig. 4. The 90% confidence limit is $\sin^2 2\theta < 6 \cdot 10^{-3}$ for $\Delta m^2 \gtrsim 20\text{eV}^2$ and $\Delta m^2 < 7 \cdot 10^{-2}\text{eV}^2$ at $\sin^2 2\theta = 1$. Ignoring all beam-related backgrounds gives the high Δm^2 90% C.L.: $\sin^2 2\theta < 8 \cdot 10^{-3}$.

Study of the data for the search for $\nu_\mu \rightarrow \nu_e$ oscillations from the LAMPF pion decay in flight neutrino beam [4,5] is in progress.

ACKNOWLEDGMENTS

The author would like to acknowledge the support and many fruitful discussions with A.K.Mann. I would also like to thank the members of the LSND collaboration and the students who worked on the project, with whom most of this work was done, and the staff of LAMPF. This work is supported in part by the U.S. Department of Energy. The material presented here is part of a Ph.D. thesis submitted to the University of Pennsylvania, which will be made available for anonymous ftp upon completion of thesis defense in early May, '95.

REFERENCES

- [1] Pontecorve, B., *Zh. Eksp. Theor. Phys.* **33**, 549 1957, translated *Sov. Phys. JETP* **6**, 429 (1958).
- [2] R. C. Allen, *et al.*, *Nucl. Instr. Methods*, **A291**, 347 (1990).
- [3] R. L. Burman, *et al.*, *Nucl. Instr. Meth.*, **A291**, 621 (1990).
- [4] Strossman, W., *A $\nu_\mu \rightarrow \nu_e$ Oscillation Search*, Ph.D. Thesis, Univ. of California, Riverside, 1995. (unpublished)
- [5] Michael Albert, *A Measurement of the Reaction $C(\nu_\mu, \mu^-)X$ Near Threshold*, Ph.D. Thesis, Univ. of Penn., 1994. (unpublished)
- [6] M. Albert, *et al.*, *Phys. Rev. C*, **51**, R1065, (1995).
- [7] J. Napolitano, *et al.*, *Nucl. Instr. Meth.*, **A 274**, 152 (1989).

FIGURES

FIG. 1. Positions of the beam-unrelated backgrounds. The scatter plots show positions of individual e^\pm (upper plots) and associated gamma rays (lower plots) in YX and YZ projection. No $e-\gamma$ coincidence is required for these samples, beside the 1ms time coincidence required by the on-line trigger. The tangent surface to the PMT faces is the plot boundary in the Y-Z projection, and the solid arcs together with the plot boundary in the Y-X projection. e^\pm are restricted to the region $d_e^{\text{PMT}} > 30\text{cm}$. The distance between centers of adjacent PMT is 35cm.

FIG. 2. Positions of the beam-on events. The 142 e^\pm shown (upper plots) are the superset from which all $e-\gamma$ coincidences must be drawn. The lower plots show the positions of the 189 gamma rays that occur in the 1ms windows these electrons have initiated. The neutrino beam is along $-0.1\hat{y} + 0.99\hat{z}$. These data represent the full 4 months (5904C) of beam.

FIG. 3. (a) The 25 beam-on $e-\gamma$ coincidences, before the application of the fiducial volume cut. The fiducial region, indicated by the dotted line, is 50cm from the PMT faces, except at the bottom of the detector, where it is 149cm from the PMT faces. Events within this volume are denoted as solid circles, while those outside are represented as open circles. This volume is 55% of the volume represented in Figs. 1 and 2. (b) The e^\pm spectrum for these 25 events. The five events passing the fiducial volume cut make up the shaded portion of the plot.

FIG. 4. Exclusion plot for mixing parameters Δm^2 and $\sin^2 2\theta$. The region to the right of and above the solid curves is excluded by this analysis at the 90(95)% confidence level. At high $\Delta(m^2)$, $\sin^2 2\theta < 6 \cdot 10^{-3}$ and at full mixing $\Delta(m^2) < 0.07\text{eV}^2$ (90% C.L.). The dash-dot curve is the result of BNL-E776, and the dashed curve is the result from KARMEN.

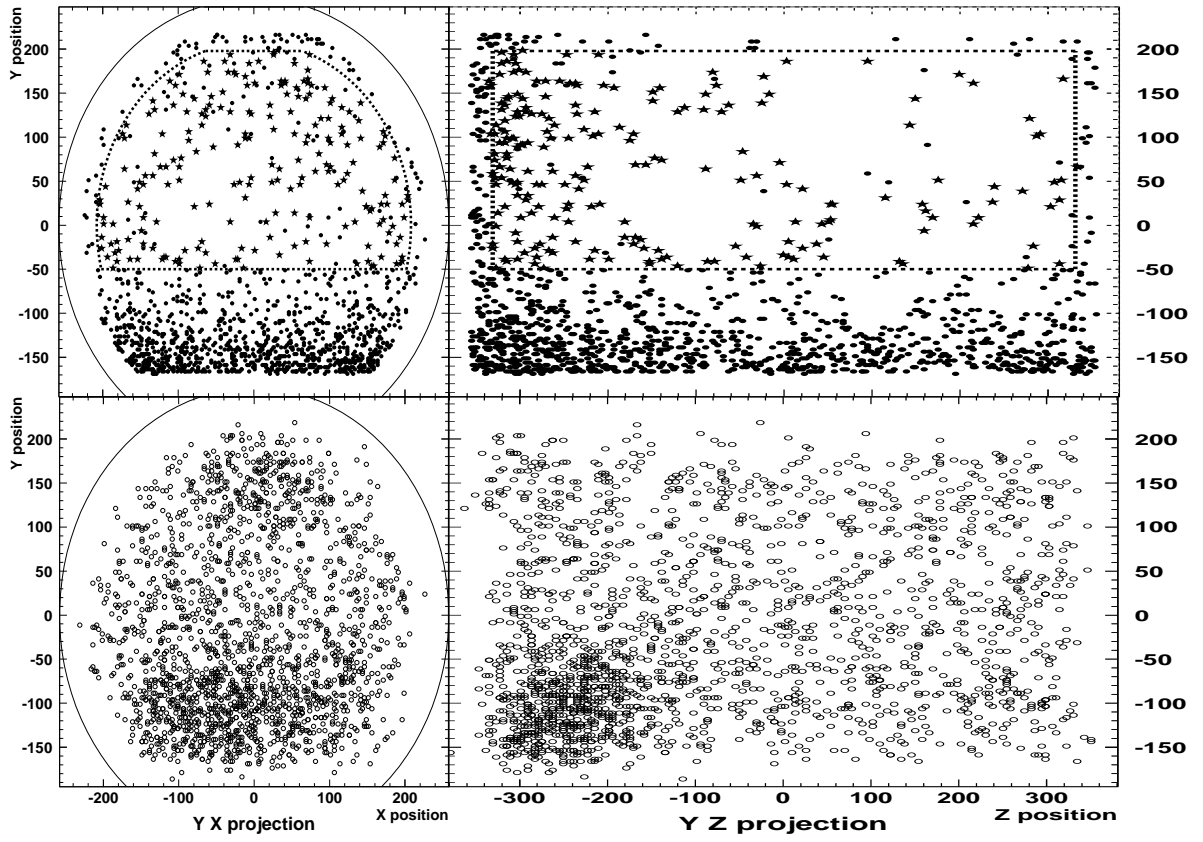
TABLES

TABLE I. Efficiency of selection for the final sample. The efficiency of in-time veto shield and previous detector activity are measured by generating external control events with a laser. The cut on previous activity of e^\pm is motivated by the large background of muon decay.

Cuts applied on	Acceptance
previous activity	0.65
in-time veto for e^+	0.87
e^+ particle ID	0.89
Live time for e^\pm	0.81
e^\pm - γ correlation	0.93
γ energy	0.9
in-time veto for γ	0.93
Live time for γ	0.78
Total	0.25

TABLE II. Expectation values for some important backgrounds. The two largest are measured (not calculated).

ν source	reaction in LSND	N_{expected}
Beam-unrelated background		3.3 ± 0.5
Beam induced e^\pm with accidental γ		2.5 ± 0.9
$\mu^- \rightarrow \nu_\mu \bar{\nu}_e e^-$	$\bar{\nu}_{e\text{p}} \rightarrow e^+ \text{n}$	0.3 ± 0.1
$\pi^- \rightarrow e^- \bar{\nu}_e$	$\bar{\nu}_{e\text{p}} \rightarrow e^+ \text{n}$	< 0.01
$\pi \rightarrow \mu \nu_\mu$ in flight	$(\bar{\nu}_\mu^-) X \rightarrow \mu \text{n} X$	0.1 ± 0.1
Total		6.2 ± 1.6



(a)

